A&A 452, 37–46 (2006)
DOI: 10.1051/0004-6361:20054050

Astronomy & Astrophysics

Determining time delay in the gravitationally lensed system QSO2237+0305

E. A. Koptelova, V. L. Oknyanskij, and E. V. Shimanovskaya

Sternberg Astronomical Institute (SAI), Moscow University, Universitetskii Pr. 13, 119992 Moscow, Russia
e-mail: koptelova@xray.sai.msu.ru; [oknyan;eshim]@sai.msu.ru

Received 15 August 2005 / Accepted 16 January 2006

ABSTRACT

Aims. We considered the possibility of measuring time delays between components of the multiplied quasar QSO2237+0305 and between V and R band variations.
Methods. The analysis is based on the flux variations of four components observed by the OGLE collaboration and Maidanak group during the last quarter of 2003. The observed gradients of the brightness variations in this period for OGLE data in V band are 3.4 mmag/day, 2.2 mmag/day, 2.4 mmag/day, and 1.1 mmag/day for the components A, B, C, and D, respectively. The variations are probably intrinsic source variations. The basic method used for time-delay measurements is the cross-correlation technique. To estimate the uncertainty of the time-delay measurements, Monte Carlo simulations were carried out.
Results. The calculations showed the impossibility of unambiguously measuring the differential time delays between the components. The observations at shorter wavelengths seem to be the only way to achieve robust time delay measurements in the system. The wavelength-dependent time delays can be used to provide the evidence of an accretion-disk structure of the central optical variable source. The observed V and R band variations of component C show good correlation with the correlation coefficient of 0.83. However, the obtained time delay, about 16.2 days, and its accuracy are far from reliable.

Key words. gravitational lensing – galaxies: quasars: individual: Q2237+0305 – methods: data analysis – cosmology: observations

1. Introduction

As was shown by Refsdal (1964), a time delay between images of a gravitationally lensed system can be used for estimating the Hubble constant and the mass distribution of the lens. At present, the time delays have been measured, at least for eleven of the lensed systems. For the particular multiple-imaged quasar QSO2237+0305, discovered by Huchra et al. (1985), a number of studies have been aimed at predicting and measuring time delays between the components of the system.

The system is very compact, about 1.8″ between the images (Yee 1988). The redshift of the lensing galaxy, $z_l = 0.039$, is low compared to the quasar redshift of $z_q = 1.7$. That leads to the small time delays between the four images – less than a day (Schneider et al. 1988; Rix et al. 1992; Wambsganss & Paczinski 1994). It means that the observed flux fluctuations uncorrelated between the images are dominated by microlensing, the first evidence of which was observed in August 1989 by Irwin et al. (1989). Since the quasar's intrinsic variations last in the hundreds of days, with time delays between the images of the order of hours, brightness variations should show up almost simultaneously and proportionally in all quasar images. However, the microlensing affects the light curves of the images differently. Thus, Østensen et al. (1996) reportedly observed an increase of about 0.6 mmag/day during 1994 in all four components. It was the only evidence of correlating variations of the components. However, the amplitude of the variability was too small for time delay measurements.

Recently the time delay of 2.7 h measured in the X-ray band between the components A and B, with component A in the lead, was published by Dai et al. (2003). Amplitudes of quasar variations in the optical band are smaller than in X-ray band and often are too small to perform cross-correlation analysis (see e.g. Giveon et al. 1999).

In the last quarter of 2003 observational period, there are 100-day variations in the components of QSO2237+0305 that are probably intrinsic to quasar. Here, we analyse the possibility of time-delay determination in the system starting from an assumption about observed quasar's intrinsic variation. Our goal here is to find out if the ground-based optical observations of the system allow time delay to be determined and, if so, with what uncertainty. In the next section, we describe the technique used for the time-delay measurement. In Sect. 3 the approach is applied to the observational data of QSO2237+0305 obtained during the ongoing OGLE monitoring programme over past eight years in V band. The photometric data were taken from `http://www.astrouw.edu.pl/~ogle/ogle3/huchra.html`. It is the most homogeneous, well-sampled, and accurate data set available for the system. To estimate the time-delay uncertainties, the computational procedure was also applied to the artificial light curves with the properties of real light curves, such as power spectrum density, observational errors, and irregular sampling.

Of some interest is detection of the time delay between two wavebands due to different sizes of quasar-emitting regions at different bands. The interband time delay can be used for independent estimation of the Hubble constant, as well as the size of the central optical variable source (Collier et al. 1999). Sergeev et al. (2005) have determined interband lags between variations in the B band and variations in the V, R, and I bands for 14 AGNs observed at the Crimean Astrophysical Observatory. The cross-correlation analysis revealed that lags range from a

tenth of a day to several days. The measured interband time delays for gravitationally-lensed systems have been published for QSO0957+561. Collier (2001) reports the time delay, $\tau = 3.4^{+1.5}_{-1.4}$ days, between the g- and r-band large amplitude variation during February – June 1996 in the lensed quasar QSO0957+561 that allows the size of the quasar emission region to be estimated. Oknyanskij (1999) reported on a possible time delay of about 230 days between radio (4 cm) and radio (6 cm) variations in QSO0957+561 and a time delay of about 6 years between the optical and radio bands. The time-delay measurements between V and R bands for the lensed quasar QSO2237+0305 are described in Sect. 6. Observational data in the R band for the same period were obtained from Maidanak Observatory (Koptelova et al. 2005).

Discussion of desirable observational parameters, which may permit successful time-delay measurements between the components of the lensed systems and between different bands, concludes this study in Sect. 7.

2. Method of cross-correlation analysis

Comparison of light curves shifted relative to each other suggests a cross-correlation analysis. A number of cross-correlation techniques are available for time-delay measurements that take into account the sampling of the data and possible contamination by sources of uncorrelated variability, such as microlensing of individual images, photometric errors, and possible systematic errors. Here, we use the technique proposed by Gaskell & Peterson (1987), which is based on linear interpolation of a data set. In the situation when the expected time delay is less than the sampling of the observational data, the interpolation or smooth fitting of the data seems to be more appropriate (see Patnaik & Narasimha 2001). However, the disadvantages are the interpolation and correlation errors. The method of Gaskell & Peterson (1987) can be improved by imposing a special restriction on the use of interpolated data: only those that are separated (in the time domain) from the nearest actual observations by no more than some fixed value $\Delta t_{\max}$ are used for cross-correlation analysis. In the approach proposed by Gaskell & Peterson (1987), the edges of the interpolated time series are extended by a constant value equal to the end magnitude values before cross-correlating. This leads to decreasing the maximum value of the cross-correlation function and does not affect the shape and position of the cross-correlation function (see Koratkar & Gaskell 1989). Here, the extension outside end points of the series bounded by the interpolation interval $\Delta t_{\max}$ was adopted. The modifications were introduced by Oknyanskij (1993). Further we call the approach MCCF (modified cross-correlation function) and state the general steps of the procedure.

Let $A(t_i)$ and $B(t_i)$ be the magnitude measurements of the two components of a gravitational lens system at time t_i. Since the data are not uniformly sampled, the linear interpolation between observations in one time series is implemented. Thus each point from time series $B(t_i)$ is correlated with an interpolated value of time series $A(t_i)$ at time $t_i + \tau$. Then each point in series $A(t_i)$ is correlated with an interpolated point at time $t_i - \tau$ in series $B(t_i)$. The cross-correlation function is calculated as follows:

$$MCCF(\tau) = \frac{1}{M} \sum_{i,j} \frac{(A_i - \overline{A})(B_j - \overline{B})}{\sigma_{\rm A}\sigma_{\rm B}}, \quad (1)$$

where M is the number of data pairs (A_i, B_j) for which $\tau - \Delta t_{\max} \leq \Delta t_{ij} < \tau + \Delta t_{\max}$ (where Δt_{ij} is the time shift between the t_i point of the A time series and the t_j point of the B time series), σ_x is the standard deviation and $\overline{x}$ is the mean of x. The final correlation coefficients, calculated twice for each value of time lag, are taken to be the average of the two. When both time series have nearly the same photometric accuracy and temporal sampling, there is no reason to favour interpolations in one time series over interpolations in the other. However, in the case when compared time series have different densities of observational points, the interpolations in the time series with the frequently-sampled observational points and accurate photometry are preferable since the interpolation errors in that case tend to be minimal. The value $\Delta t_{\max}$ is chosen so as to provide the compromise between the desire to decrease the interpolation errors and to seek consistency with the characteristic time of intrinsic quasar variations. If we choose $\Delta t_{\max}$ too small, we may be unable to find a sufficient number of pairs of points to reliably calculate the correlation coefficient for a given lag. Too large a value of $\Delta t_{\max}$ causes an increase in the interpolation errors and decrease in the resolution of the method that is characteristic of the method proposed by Gaskell & Peterson (1987). Another distinctive feature of the MCCF approach is the different number M of pairs of points used to calculate the correlation coefficient for various lags, i.e. M cannot be too small. The values obtained for $M < 10$ are therefore excluded. Besides, the correlated measurement errors can lead to a spurious minimum at zero lag, since these errors are equal on the same day. Thus the correlated errors can be important if the correlation peak is expected near zero lag (see Gaskell & Peterson 1987; Koratkar & Gaskell 1991). To avoid their influence, the points of the time series $A(t_i)$ should be correlated with the points of the time series $B(t_j)$ for which $t_i \neq t_j$. This was taken into account in the modified version of the MCCF approach.

The MCCF method has been successfully implemented for time-delay determination between the images of QSO0957+561 (Slavcheva-Mihova et al. 2001), for the time-delay measurements between near-IR, optical, and UV variations for several AGNs (see Oknyanskij 1999) and for time-delay measurement between the continuum and line variations of NGC 4151 (Oknyanskij et al. 1994). The published results clearly show the stability and robustness of the method.

We can also represent the quasar variations by a smooth function for one of the images. The polynomial fitting of the data set can introduce additional shifts that are undesirable for measuring such short time-delays. Since the higher the order of the polynomial the higher is its oscillations. Instead we use spline interpolation and regularized fitting (Tikhonov & Arsenin 1977) of the data set. The correlation function in this case can be represented as follows:

$$SCCF(\tau) = \frac{1}{M} \sum_{i} \frac{(f_{\rm A}(t_i + \tau) - \overline{f_{\rm A}})(B(t_i) - \overline{B})}{\sigma_{f_{\rm A}}\sigma_{\rm B}}, \quad (2)$$

where $f_{\rm A}(t)$ denotes smoothed time series.

In Sects. 3 and 6 we present the results of time-delay calculations with the described approaches.

3. Application to the gravitational lens system QSO2237+0305

We are primarily interested in testing the particular case of QSO2237+0305. Despite extensive optical monitoring programmes carried out at the Nordic Optical Telescope (Østensen et al. 1996) within the OGLE programme (Woźniak et al. 2000), by the GLITP collaboration (Alcalde et al. 2002) at the Apache Point Observatory (Schmidt et al. 2002), and at Maidanak

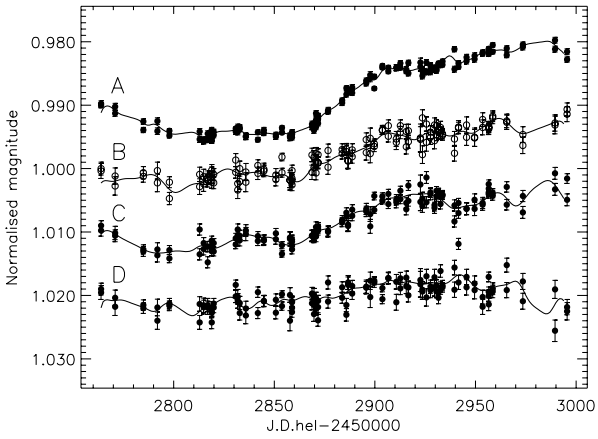

Fig. 1. The V band light curves of the A−D components of QSO2237+0305 from day 2763.91 to day 2995.54 from OGLE observational data. Solid lines show the regularized fitting to the observational data.

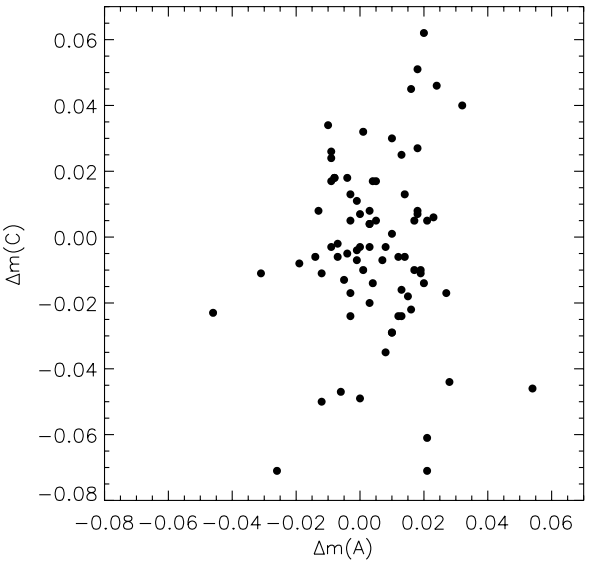

Fig. 2. Differences in the magnitudes of the components A and C for pairs of observations that are separated by no more than 1 day.

Observatory (Bliokh et al. 1999; Dudinov et al. 2000; Vakukik et al. 2004), there was no significant intrinsic variability detected in QSO2237+0305. The macrolens models of the system predict the time delays of about one day for all components, so the intrinsic variations in the source should manifest themselves almost at the same time in all four images. The amplitude peak-to-peak variations for all components should vary by the same value. However, detecting the correlated variations for QSO2237+0305 is complicated by the high microlensing activity of the system.

The variability of component A with an amplitude of about 0.2 mag is clearly seen in Maidanak observational data over the last quarter of 2003 period (Koptelova et al. 2005). Observations carried out by the OGLE collaboration with more accurate photometry and denser sampling revealed that the same feature is also present in those components B and C of the system with amplitudes about 0.15 mag. The gradients of the brightness variations for the period from day 2850 to day 2900 are 3.4 mmag/day, 2.2 mmag/day, 2.4 mmag/day, and 1.1 mmag/day for the components A, B, C, and D, respectively. The drop in light curves of the A−C components follows this rise. These are several times more rapid brightness variations than reported by Østensen et al. (1996) for the correlated brightness variations observed in 1994. Observations of QSO2237+0305 variability during the period under consideration do not show microlensing activity with special events. Later OGLE observations gave evidence of component B microlensing variability, but we do not consider it in this work. Figure 1 shows the light curves of A−D images of QSO2237+0305. Solid lines are the result of the fitting procedure of the data with a regularization technique. The light curves were first normalized by dividing by the magnitude value of the first epoch and than shifted along vertical axes relative to each other. As illustrated in Fig. 1, the similar variability of components A−C during the analysed epoch can be interpreted as an intrinsic variability of the quasar. However, the variability due to superposition of microlensing and intrinsic quasar activity cannot be excluded. Component D of the system is weak enough and its photometry is a rather difficult task. Image D is located near the brightest image A, so it suffers from large photometric uncertainties. Besides, its variation per day is at least two times smaller than for other components. Hence, we cannot come to any conclusion about the variability of the image D from these observational data, so we focus on the OGLE observational data for the components A−C of the system from day 2763.91 to day 2995.54. This period is characterised by a high temporal resolution. In order to determine time delays, we used methods based on a cross-correlation technique with: (1) linear interpolation in the temporal domain (the method of Gaskell & Peterson 1987; with modifications of Oknyanskij 1993); (2) cubic spline smoothing; (3) regulirized fitting of the observational data.

The data under analysis are characterised by the mean standard errors of observations $\sigma_A = 0.007$ mag, $\sigma_B = 0.017$ mag, $\sigma_C = 0.015$ mag, and $\sigma_D = 0.020$ mag. A set of correlation coefficients can be derived from a set of lags. The maximum of the correlation function is supposed to be the best solution for the time delay. This way the estimation of time delays of the images B and C with respect to image A and between images C and B were carried out. Since the data were calibrated with the nearby reference star, errors in determining its flux from night to night could affect the fluxes of the components in the same way. In order to determine the effect of correlated errors, the observational data obtained in the same night for AB, AC, and CB pairs of the components were compared. It was found that the data for compared pairs did not show any evidence of large correlated errors. An example of magnitude differences for the components A and C that are separated by no more than 1 day is presented in Fig. 2. The scatter of the points are mainly due to the measurement errors.

Some observational points can influence the result and their removal can change the maximum of the correlation function. Thus the more stable cross-correlation estimates of the time delay should be undertaken. For this purpose the points chosen by chance were removed from the discrete time series. It can give a bootstrap estimate of the time-delay uncertainty. The position of the maximum value of the cross-correlation function (median value, parabolic fit, or actual) corresponds to the time delay.

We began our analysis from the correlation of the A and C light curves, as their signal-to-noise ratios are larger then for the fainter component B. The cross-correlation approach with linear interpolation of one of the time series described in Sect. 2 was applied to the observational data. The light curve of the component A was used for the interpolation as it has the best photometric accuracy. The time-shifted and interpolated A light curve

and the discrete C light curve are compared with each other. Since the expected time delay for the system is about one day, the time resolution of 0.1 day with the bin size of 1 day was adopted. The maximum of the cross-correlation function corresponds to the time delay $\tau_{\rm CA} = -50.4$ h. Here and later the negative value of τ_{XY} means that variations in image Y follow variations in image X, and vice versa. The stability of the obtained result was proved with calculations where the points chosen by chance were removed from the observational sequence of C data set. Thus, we can roughly estimate the time delay of $-50.4^{+115.2}_{-57.6}$ h (95% confidence level). This estimation was found taking the actual maximum value of the cross-correlation function. But the correlation function can have several peaks located around small lags. Thus, the problem of finding a single value that corresponds to a definite lag appear. Then to find the maximum value, the least-square parabolic fit in the lag range near the maximum of the cross-correlation function can be used (Lehár et al. 1992). To find time delay between components C and A, the part of the correlation function corresponding to $[-10, 10]$ days time interval was fitted. The best solution found for the time delay equals -117.6 h. Additional peaks can also be damped out by increasing the bin size. Thus we get more data pairs to be averaged over and the correlation function tends to be smoother. This leads to excluding those high frequencies that can contain the required signal from the cross-correlation function. The actual maximum in all cases is located around zero lag. It makes time-delay measurements to an accuracy of hours with an intraday time resolution difficult. The cross-correlation functions calculated for the AB, AC, and CB pairs of the components are presented in Fig. 3 (black curves). As can be seen, they are slow variable functions with several peaks on their maximum.

Then we proceed with the assumption that quasar brightness variations can be represented by a smooth function. The cross-correlation function in this case is smoother and the result is less sensitive to bias produced by additional peaks. Thus, the calculations were repeated with the spline-fitted A light curve. Another way to construct smooth light curves is a fitting of the noisy and non-uniformly sampled data by means of regularization technique (Calvini et al. 1995). The results of the fitting are shown in the Fig. 1 by the solid lines. The mean squared deviations of the smoothed time series and observational time series are 9.9 mmag, 1.2 mmag, 19.7 mmag, and 1.4 mmag for the A, B, C, and D components, respectively. Figure 3 (faint curves) shows the cross-correlation functions calculated for the AB, AC, and CB pairs of the components with one of the curves smoothed. The time delays obtained with the cross-correlation technique for interpolated and smoothed data are tabulated in Table 1. In these computations, detrending that can be caused by microlensing was not taken into account.

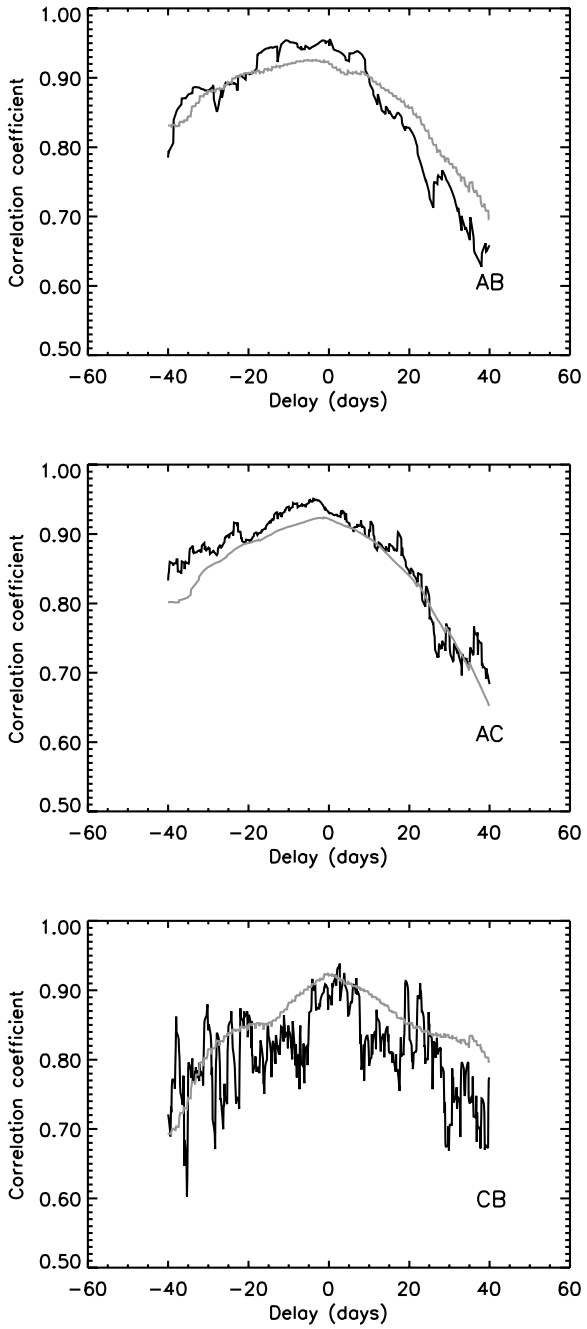

Fig. 3. Cross-correlation functions for the AB, AC, and CB pairs of the components obtained with linear interpolating (black curves) and regularized fitting (faint curves) of the observational data.

4. Study of uncertainties

To estimate errors of time delay determination, the cross-correlation approach described in Sect. 2 was applied to simulated data with the specified time delay. The proposed techniques for time-delay determination show robustness for the situation when duration of intrinsic quasar variations and/or observational sampling are much less than the expected time delay. It is desirable to simulate light curves with the statistical properties of the observed light curves. One of the ways to do this is to simulate the light curves from the real data (see e.g. Pelt et al. 1996). The robustness of the method can be demonstrated by comparing the light curves with some points removed by chance. The estimations of time-delay uncertainties in this case can be even better than from simulated light curves (see Sect. 3). It means that not all statistical properties are incorporated into the simulated light curves. In this section, the robustness of the approaches described in Sect. 2 is tested and time delay uncertainties are determined from the synthetic light curves.

4.1. Generating light curves

Since QSO2237+0305 itself did not show any unusual behaviour over the period of observations, the quasar can be referred to the family of those quasars with average statistical properties. The artificial light curves are supposed to reflect the real intrinsic variability of the quasar. Much attention is paid to the

Table 1. Time-delay estimations (hours) between images B-A, C-A, and B-C. The uncertainties obtained from Monte Carlo simulations correspond to a 95% confidence level.

Method	τ_{BA}	τ_{CA}	τ_{BC}
interpolation	$-76.8^{+146.4}_{-96.0}$	$-50.4^{+132.0}_{-120.0}$	$64.8^{+302.4}_{-72.0}$
parabolic fit	$2.4^{+81.6}_{-259.2}$	$-117.6^{+38.4}_{-96.0}$	$52.8^{+168.0}_{-117.6}$
spline smoothing	$14.4^{+112.8}_{-96.0}$	$-57.6^{+84.0}_{-79.2}$	$26.4^{+48.0}_{-69.6}$
regularizing fit	$-43.2^{+151.2}_{-108.0}$	$-36.0^{+148.8}_{-105.6}$	$-4.8^{+240}_{-124.8}$

statistical properties of the observed quasar light curves over long time intervals. A number of studies are dedicated to investigating quasar variability properties based on monitoring individual quasars. The structure function analysis and power spectrum analysis are both used for measuring the power distribution over time. The structure function is a common statistical tool used to analyse the variability properties of quasars. To analyse the quasar structure function, the long-time scale observations of a large sampling of quasars are needed. Hook et al. (1994) published studies based on the variability properties of about 300 optically-selected quasars observed during 16 years. It enabled the variability as a function of time interval to be determined and models of quasar variability to be tested. One of the models was applied to the simulation of artificial light curves in the paper by Eigenbrod et al. (2005) dedicated to observational strategies for the time-delay measuring between the images of gravitationally-lensed quasars. De Vries et al. (2005) employ much larger database of quasars and show that the structure function should be modeled in a more complicated way, and that at least two variability components are needed.

Another method of light-curve simulation is an inverse Fourier transformation of a model quasar's power spectrum with power-law index α. The optical data can be modeled as a power law with a mean index $\alpha \simeq -1$ (see Zheng et al. 1997). Timmer & König (1969) proposed an algorithm that is able to produce the variety of time series that exhibit a $(1/f)^{\alpha}$ spectrum. This method allows randomizing of both the phase and the amplitude of the Fourier transform of the data. We used this method to simulate light curves for a power spectrum that is an inverse function of a frequency. The method has two steps. For the given set of Fourier frequencies $\{\omega_i\}$ and a power spectrum with a given power law, real and imaginary parts of the Fourier transform are calculated as follows:

$$f(\omega) = N(0,1)\sqrt{\frac{1}{\omega}} + iN(0,1)\sqrt{\frac{1}{\omega}}, \quad (3)$$

where $N(0,1)$ is a normally distributed stochastic variable with zero mean, and the standard deviation equals one. Then the simulated light curve is obtained by applying the inverse Fourier transform and renormalizing the light curve to the observed magnitudes. The artificial light curves are resampled as the observational ones. The second light curve is obtained by adopting the time delay τ. To simulate the measurement noise, the normally distributed variable with zero mean and standard deviation matching the actual measurement uncertainties was added to the simulated data set. Figure 4 shows an artificial light curve with the data points selected in a single Monte Carlo simulation and its power spectrum calculated as proposed by Deeming (1975).

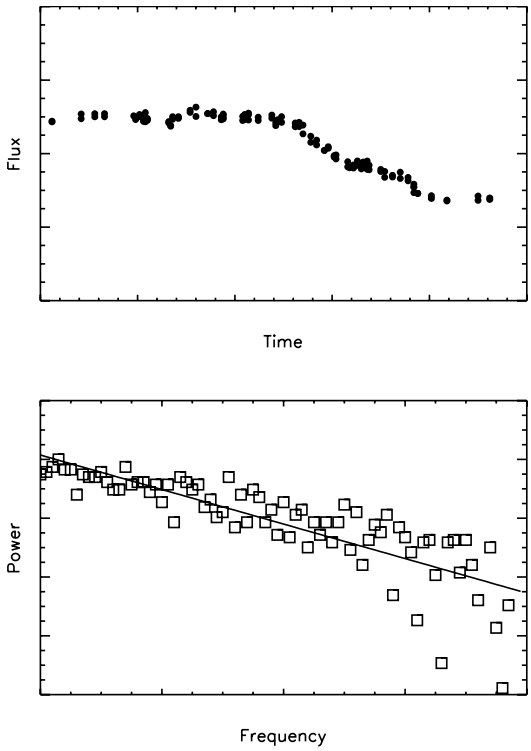

Fig. 4. The *top panel* shows the model light curve, generated from a power-density spectrum $P(f) \sim 1/f$ with the data points selected in a single Monte Carlo simulation. The bottom panel shows its power spectrum.

4.2. Monte Carlo simulations

In the simulations both time series have N points sampled at the same time, which is characteristic of OGLE data. The N selected data points from each series are then cross-correlated as if they were real data. The interpolation step is set equal to 0.1 day. The time delays obtained with a cross-correlation method in the case of linear interpolation, spline smoothing, and regularized fitting are recorded and used to build distribution functions. After 1000 realizations, each particular distribution function is integrated to determine the probability that a given realization yields a result above the specified threshold value. Distributions of time delays recovered from cross-correlation analysis with linear interpolation of Monte Carlo simulated light curves are shown in Figs. 5–7. The bin width is set to 1 day to visually represent the cross-correlation peak distribution. These distributions are almost always non-normal and the standard deviation of the distribution is not a good representation of the time-delay uncertainty. The results of the tests are summarised in Table 1. The uncertainties $\Delta\tau^{-}_{95}$ and $\Delta\tau^{+}_{95}$ quoted in Table 1 are computed directly from the distribution and defined such that 95% of the realizations yield results within $[\tau-\Delta\tau^{-}_{95}, \tau+\Delta\tau^{+}_{95}]$ or, its equivalent, which is that 5% of the realizations fall outside that interval. It corresponds to 2σ errors for the normal distribution.

4.3. Observational parameters

The accuracy of the time-delay determination depends strongly on the temporal sampling except for the photometric accuracy, amplitude of quasar variation, and microlensing influence. As shown by many authors, the photometric treatment of the lens QSO2237+0305 is a challenging task, as the quasar images overlap due to compactness of the system. The situation is

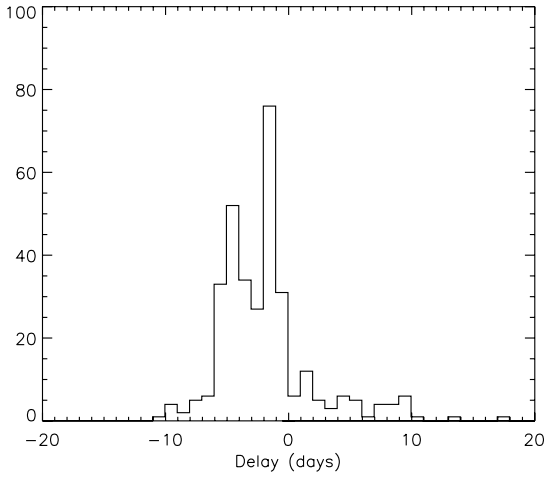

Fig. 5. Distribution of time delays recovered from cross-correlation analysis of 1000 Monte Carlo simulations of the A and B light curves.

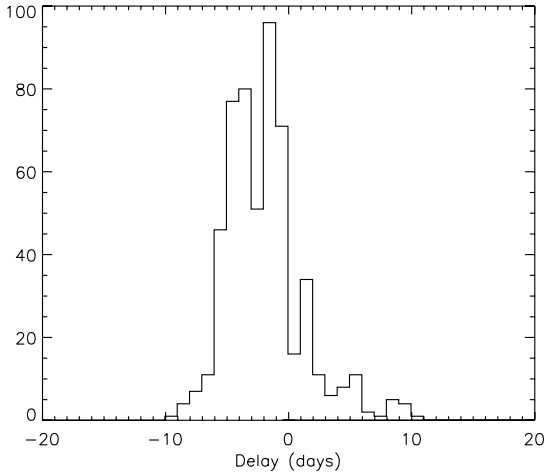

Fig. 6. Distribution of time delays recovered from cross-correlation analysis of 1000 Monte Carlo simulations of the A and C light curves.

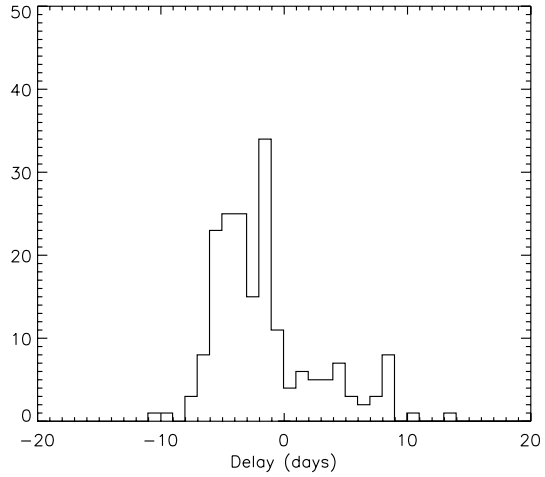

Fig. 7. Distribution of time delays recovered from cross-correlation analysis of 1000 Monte Carlo simulations of the C and B light curves.

complicated by the presence of the bright underlying galaxy. Thus, the achieved photometric accuracy in optics from ground-based observations is unlikely to be improved. Can the temporal sampling be properly adjusted to extract such short time delays? To answer this question, the numerical simulations with artificial

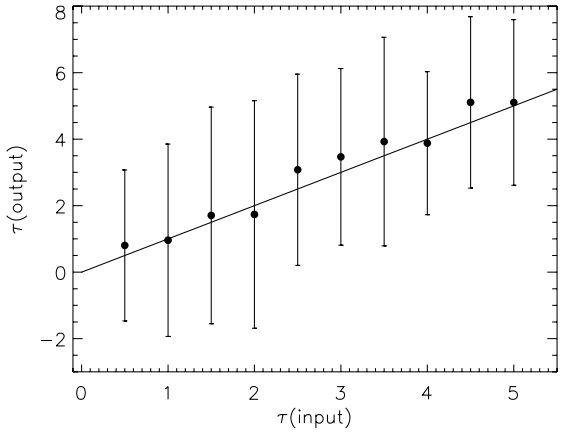

Fig. 8. Time delay $\tau_{\rm out}$ (days) determined by the cross-correlation method as a function of the true time delay $\tau_{\rm in}$ (days). The uncertainties have been estimated using 100 simulated light curves with the same temporal sampling and errors as observational data for components A and C.

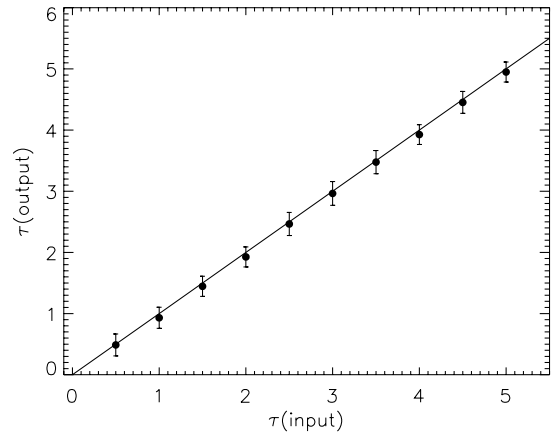

Fig. 9. Time delay $\tau_{\rm out}$ (days) determined by the cross-correlation method as a function of the true time delay $\tau_{\rm in}$ (days). The uncertainties have been estimated by using 100 simulated light curves for the regularly-spaced sampling intervals of 1 day and with the same observational errors as observational data for components A and C.

quasar light curves were used. We consider only the time delay between the brightest images of the system. Adopting the achieved photometric accuracy, amplitudes of observed variations and observational sampling for the components A and C (see Sect. 3), the time delay $\tau_{\rm out}$ determined with the cross-correlation method as a function of the true time delay $\tau_{\rm in}$ was calculated (see Fig. 8). The uncertainties were estimated by using 100 light curve simulations. Figure 9 shows the results of the calculations for the regularly-spaced sampling intervals of 1 day with observational errors as for components A and C. As can be seen from Figs. 8 and 9 the temporal sampling of observations has a strong influence on the uncertainties of the time-delay determination. The good accuracy of time-delay determination should be able to be achieved, but with well-sampled monitoring observations that are difficult to organize.

4.4. Microlensing influence

The microlensing variations can act on the same time scale as intrinsic quasar variations. The variations due to microlensing were clearly detected in four components of QSO2237+0305. As noted in Sect. 3, the variability due to summation of

Table 2. Predicted time delays (h_{75}^{-1} h) for QSO2237+0305. The time delays obtained from the best fit models are quoted.

Reference	Δt_{BA}	Δt_{CA}	Δt_{DA}
Schneider et al. (1988)	–0.54	6.48	6.12
Rix (1992)	–1.3	7.4	2.8
Wambsganss & Paczynski (1994)	–0.44	2.54	0.7
Schmidt et al. (1998)	–2.0	16.2	4.9

microlensing and intrinsic quasar activity cannot be excluded from consideration. Thus, the influence of the microlensing on time-delay measurements should be estimated.

The first approximation of the microlensing variability can be simulated by adding a linear trend to the artificial quasar light curve. The observed difference in the amplitude of variations for the components A and C is about 0.05 mag, which can be caused by slow microlensing variability. To model it, the linear trend with gradient of 0.25 mmag/day was added to one of the simulated light curves with a regular temporal sampling. The amplitude of the variation in the first curve was adopted as equal to 0.15 mag and the resulting amplitude of the second light curve with the small systematic microlensing was 0.20 mag.

The calculations revealed that slow linear microlensing trend of 0.25 mmag/day leads to an increase in the uncertainty of the time-delay determination in several times and a time-delay bias – up to 0.4 days. The situation for the sparsely-sampled data is even worse and reliable determination of time delay in this case seems to be impossible.

5. Predicted time delays

After the system was resolved into the four point sources residing very close to the centre of the spiral galaxy, a model of the lensing galaxy based on the observed light distribution of the deconvolved galaxy was proposed by Schneider et al. (1988) (see Erratum). According to this model, maximum time delay is expected between B and C images, with image B leading. The HST observations of the system allowed Rix et al. (1992) to get the improved model of the lens based on the same assumption about constant mass-to-light ratio. Given the positions of the components, three parameters (scaling factor for the galaxy and the quasar position) were fitted. The fit, reproducing the observable positions, was achieved with only one free parameter describing the lensing galaxy. As with the model of Schneider et al. (1988), maximum time delay was expected for the components B and C of the system. Wambsganss & Paczyński (1994) modeled the lens with the power-law mass distribution with an external shear. Their model allowed reproducing the image positions with the accuracy factor four times more precise than the constant mass-to-light model. According to their calculations the intrinsic variations of the quasar have to show up first in image B, then in images A, D, and C. A maximum time delay was also expected between B and C images. A more complicated model that takes into account the bar of the galaxy that contributes to the lensing effect was proposed by Schmidt et al. (1998).

The model-predicted time delays are combined in Table 2. As seen from the table, predicted time delays depend on the galaxy model used. Measured time delays differ considerably and cannot be used for discriminating between the existing macrolens models. Moreover, the lags are so small that observational data do not allow the sign of the time delay to be determined correctly (see Table 1).

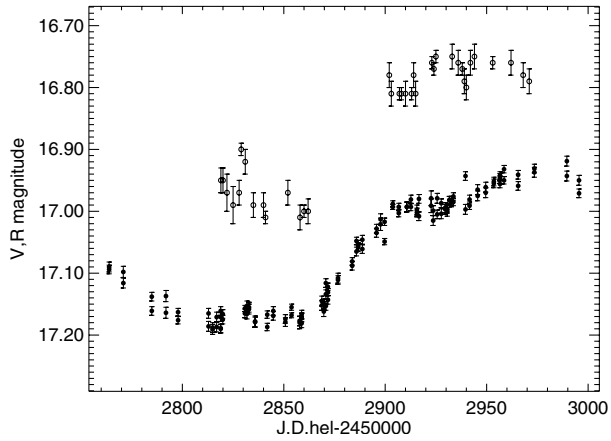

Fig. 10. Photometry of component A of Q2237+0305 in the *R* band from observations with the 1.5-m Maidanak telescope (*upper light curve*) and in the *V* band obtained by OGLE collaboration (*lower light curve*).

6. Time delay between *V* and *R* band variations

Since the different spectral bands, from X-ray to infrared, in AGNs show correlated variations in flux, the possibility of measuring time delay between light curves in two bands can be explored. According to the thermal reprocessing hypothesis, the UV/optical continuum variations of the active galactic nuclei represent the response of the accretion disk material to the variations in the central high-energy continuum. It means that X-ray radiation illuminates the surrounding gas and has reprocessed it into optical photons in an accretion disk (e.g. Edelson et al. 1996). In the standard accretion disk model, the radial temperature is $T \propto R^{-3/4}$ (Shakura & Sunyaev 1973). Radiation of a wavelength λ from the central region of the accretion disk arrives at radius R with temperature $T = hc/(k\lambda X)$ ($X = 3 \div 4$ for a black body model) after time $\tau = R/c$. Thus for a disk with $T \sim R^{-3/4}$, the time delay is wavelength dependent as $\tau \sim \lambda^{4/3}$. The observed variations at shorter wavelengths are expected to appear previous to variations at longer wavelengths.

The *R* photometric data published by Koptelova et al. (2005) was observed at Maidanak Observatory, and data in *V* band was obtained by OGLE collaboration. To determine the possible time lag between the *V* and *R* bands, the cross-correlation technique described in Sect. 2 was applied. We focus our analysis on the same time period as before. The Maidanak data are characterized by larger photometric errors, especially for the fainter B and D components of the system. Thus we restrict our analysis to components A and C. Since the Maidanak data have a significantly larger scattering of points, data points with errors of 4−5 per cent and points with the scattering correlated with the reference star were excluded from the analysis. Figures 10 and 11 show the *R* and *V* light curves of components A and C, respectively. The light curves from Maidanak Observatory are shifted arbitrarily along vertical axes. While a small inconsistency between two data sets exists, they show good agreement in the overlapping period. The cross-correlation functions for the A Maidanak light curve and A OGLE light curve and for the C Maidanak light curve and C OGLE light curve are shown in Fig. 12. A linear trend has been removed from the light curves prior to computing the cross-correlation function to account for the possible presence of slow-microlensing variations. It allows the cross-correlation analysis to be improved. For component A, the cross-correlation function is a slow variable function that has several local peaks on its maximum. The maximum

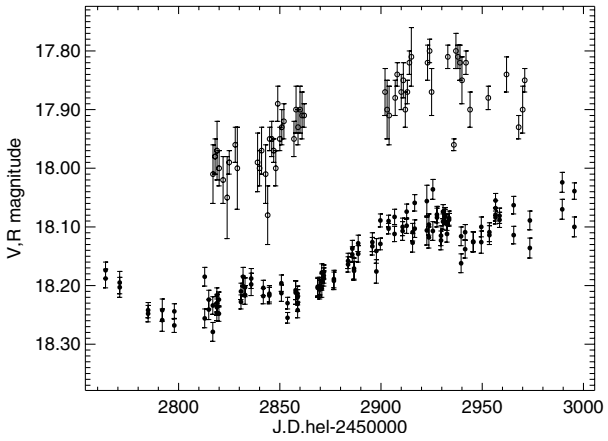

Fig. 11. Photometry of component C of Q2237+0305 in the *R* band from observations with the 1.5-m Maidanak telescope (*upper light curve*) and in the *V* band obtained by OGLE collaboration (*lower light curve*).

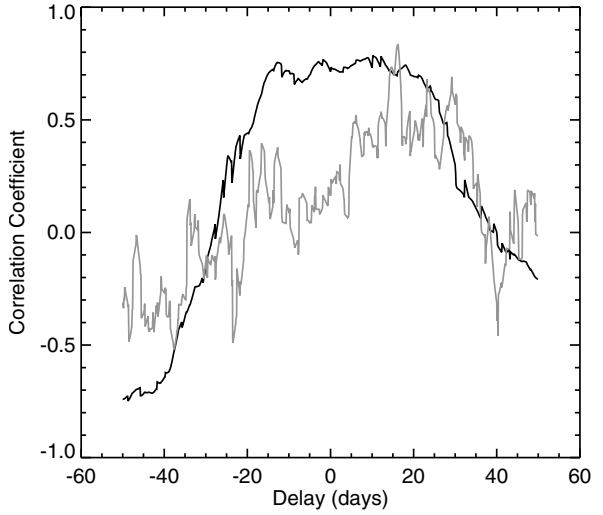

Fig. 12. Cross-correlation function calculated for the *R* band and *V* band photometrical data of component A (dark curve), and for the *R* band and *V* band photometrical data of component C (faint curve).

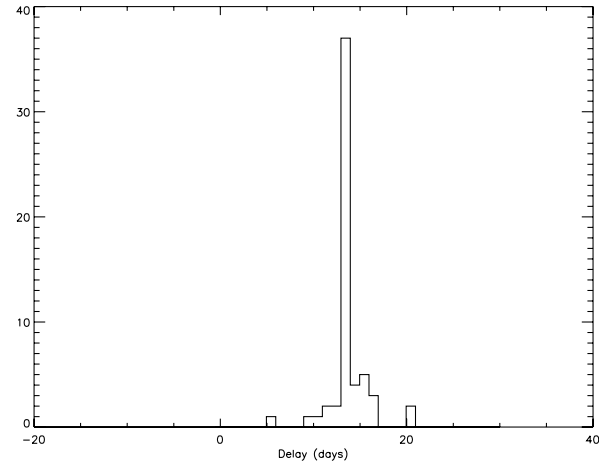

Fig. 13. Distribution of time delays recovered from cross-correlation analysis of the component C observational data with points removed by chance from the Maidanak light curve.

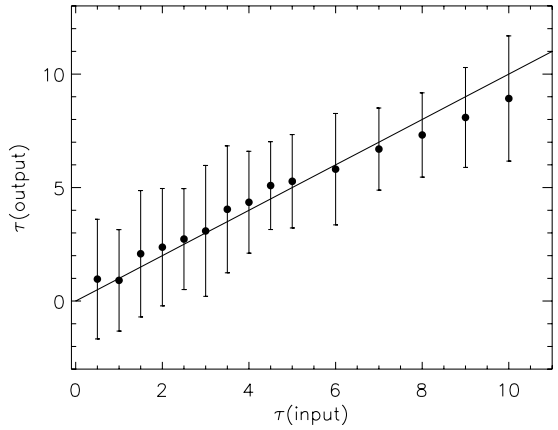

Fig. 14. Time delay $\tau_{\rm out}$ (days) determined by the cross-correlation method as a function of the true time delay $\tau_{\rm in}$ (days). For the light-curve simulations, the regular sampling and observational errors as for OGLE A and C light curves were adopted. The uncertainties have been estimated by using 100 simulated light curves distorted by linear microlensing trend.

value of the cross-correlation coefficients corresponds to 0.84. Its median value, which was computed for function values larger than 0.7, corresponds to a 9.0 day lag with *V* band variations leading. For component C, the cross-correlation function has a clearly seen peak corresponding to 16.2 days with a correlation coefficient 0.83. The Maidanak data for component C are characterized by the mean standard errors of observations $\sigma_{\rm C} = 0.033$ mag. Only several per cent of 1000 Monte Carlo simulated light curves with the statistical properties of the real light curves have a maximum of the cross-correlation function that is larger than 0.5. Thus, to estimate the stability of time-delay measurement, a set of points was removed by chance from the Maidanak light curve. The time delay and its uncertainty (95% confidence level) determined in this way is $\tau = 13.8^{+6.4}_{-4.5}$ days. Figure 13 shows the distribution of time delays recovered from the cross-correlation analysis. Although the photometric data in two bands have different observational time spans and temporal samplings, excluding the appearance of the correlated errors due to observations on the same days, another possible systematic error that would produce a peak in the cross-correlation function near zero lag is a microlensing variability. Since the microlensing variations occur without a shift in time, it will affect both optical bands in the same way. To investigate the effects of such errors, the simulated light curves distorted by a microlensing trend of 0.25 mmag/day were compared (see Sect. 4.4). The statistical properties of OGLE A light curve were adopted for simulations. The time delay was allowed to vary from 0.5 to 10 days and 100 Monte Carlo simulated light curves were produced for each time delay value. The estimates of time delay as a function of the true time delay are shown in Fig. 14. As can be seen, the presence of a slow microlensing trend leads to increasing the uncertainty in time-delay determination as in the case of larger photometric errors (see Fig. 8). The mean value of the calculated time delay decreases starting from certain value of input time delay. It is obviously due to the presence of correlated errors caused by microlensing variations. And we can conclude that for an expected time delay larger than certain value (6 days in our case) the effect of correlated errors can lead to underestimation of the time-delay value. Thus, the microlensing of image A can lead to a biased interband time delay estimate.

These results cannot pretend to determine the time lag between *V* and *R* bands as the compared data sets have much different accuracy. But they provide evidence of the presence of a

non-zero lag. Assuming that the time delay is the same as for the QSO0957+561 (Collier 2001) and taking the redshift into account, the time delay value is expected to be several days.

7. Conclusions

Robust measuring of time delays between images of the gravitationally-lensed systems is a rather difficult task. To be successful with these studies, the source needs to be variable and the observational sampling needs to be at least of the order of a time delay. Many quasars have been found to exhibit nonregular optical variations a fraction of a magnitude over a time scale from hours to days. However, most quasars have much more quiescent variability properties, changing their brightnesses up to a few tenth of a magnitude per year (e.g. Giveon et al. 1999; de Vries et al. 2005). As a rule, measuring time delays requires long-term monitoring of gravitationally-lensed systems.

Detecting short time delays between the images of the lens is rather problematic, particularly in the optical band. The sampling density of optical light curves is low and the photometric errors are large for detecting time delays of about a day. The measured time delays presented in Table 1 are rather unreliable. Those time delays cannot be used even for discriminating between the models of the lensing galaxy and for constraining the amount of dark-matter substructure in the lensing galaxy, as well as for accurate determining the Hubble constant.

As we have noted above, our analysis was performed to find out: (1) the possibility of measuring time delays between the images of the gravitationally lensed system QSO2237+0305 using optical observational data; (2) the possibility of detecting the time delay between two optical bands; (3) the uncertainty of time-delay measurements.

Employing a cross-correlation technique, we calculated time-delay estimates for complete observational light curves and for light curves with the points removed by chance. Confidence intervals (95% confidence level) were found using simulated light curves with the same sampling and errors as for observed light curves. Using the cross-correlation analysis, we showed that available ground-based observational data allow us to determine differential time delays between the images of QSO2237+0305 with rather high uncertainties. The time-delay estimations carried out with different cross-correlation approaches are in poor agreement with each other (see Table 1) and do not allow time delays to be determined between the components. There is evidence of this nonzero time delay between components A and C. As these are the brightest components of the system with the most accurate photometry, the measured time delay can be considered as a marginal result. However, even a microlensing trend of 0.25 mmag/day can yield a time-delay bias – up to fraction of a day. For the AB pair, the time delay is probably too small to be detected from the present data. For the CB pair, the photometrical accuracy and observational sampling apparently do not allow this time-delay determination. Thus, we conclude that time-delay estimations cannot be unambiguously determined for this system from today's ground-based optical data.

The observations analysed are frequent enough but have rather different photometric accuracy for the components. As noted by many researchers, the accurate photometry of QSO2237+0305 is complicated by its compactness and the presence of the bright-lensing galaxy. Thus the effects of the seeing and systematic errors connected with galaxy model subtraction can influence the results of the photometry. At the same time, detecting low-amplitude variability requires very accurate photometry. For observations with seeing worse than one arcsecond, it is very difficult to disentangle the four quasar images. Thus observations with seeing conditions better than one arcsecond are preferable.

With $M_B \approx -25$ mag, QSO2237+0305 belongs among the brightest quasars in its redshift. The quasar surveys show that high-luminosity quasars vary less than low-luminosity ones (e.g. de Vries et al. 2005). The variations that are well seen over a night in a source with low luminosity can require much longer to be detected than in a highly luminous source. As was reported by Vakulic et al. (2004), no rapid (night-to-night and intranight) photometric variations were found in the four quasar images. In addition, considering the high redshift of the quasar, the variations must be extended in time by a correction factor $(1 + z_q)$.

In the optical waveband, the variability is fairly slow, so it can only be studied with long-term, well-sampled monitoring observations. Besides, there must be a chance to observe the intrinsic variability. But the probability of observing the variability with high-amplitude events due to accretion-disk instabilities is virtually zero. Then why should we wait for this highly improbable event? The characteristic time of the variations in the X-ray band is of the order of hours as a result of the smaller size of the X-ray source. It makes it possible to detect time delays in X-rays, and OSO2237+0305 has been observed in the X-ray band. Although the results of observations with ROSAT reported by Wambsganss et al. (1999) did not show any variability intrinsic to the quasar, Dai et al. (2003) report about source variability over both long and short time scales. The X-ray flux has dropped by 20% between the two observations carried out in September 2000 and in December 2001. The cross-correlation analysis allowed measurement of the time delay between the components A and B. The measurement of the time delays between other images can allow the mass distribution of the lensing galaxy to be constrained. Thus, analysis of observational data for shorter wavelengths seems to be the only way to get robust time-delay measurements.

We also explored the possibility of detecting a time lag between two optical bands due to reverberaton within an accretion-disk structure. Higher energy radiation from the central source drives variations at longer wavelength originated in the disk. Thus the time lag between two optical bands can provide an estimate of the size of the central optical variable source. Trying to explore that possibility, we arrived at the conclusion that probably there is a nonzero lag between the two optical bands. Applying the cross-correlation technique, we found the time lag of 16.2 days with a correlation coefficient of 0.83 between the V and R band variations. However, for the robust measurment of the interband time delay, accurate and well-sampled multiband observations of the system are needed.

Acknowledgements. The authors would like to thank Dr. Boris Artamonov for many useful discussions and comments. Also we would like to thank the OGLE collaboration for making data publicly available.
This research was supported by Russian Foundation for Basic Research (RFBR) grant 06-02-16857.

References

Alcalde, D., Mediavilla, E., Moreau, O., et al. 2002, ApJ, 572, 729A
Bliokh, P. V., Dudinov, V. N., Vakulik, V. G., et al. 1999, Kin. & Phys. Cel. Bodies, 15, 338
Burud, I., Stabell, R., Magain, P., et al. 1998, A&A, 339, 701
Calvini, P., Bertero, M., & Brown, J. C. 1995, Inverse Problems, 11, 79
Collier, S. 2001, MNRAS, 325, 1527
Collier, S., Horne, K., Wanders, I., et al. 1999, MNRAS, 302, 24
Dai, X., Chartas, G., Agol, E., et al. 2003, ApJ, 589, 100
Deeming, T. J. 1975, Ap&SS, 36, 137
de Vries, W. H., Becker, R. H., White, R. L., & Loomis, C. 2005, ApJ, 129, 615

Dudinov, V. N., Vakulik, V. G., Zheleznyak, A. P., et al. 2000, Kin. & Phys. Cel. Bodies, 16, 346
Edelson, R. A., Alexander, T., Crenshaw, D. M., et al. 1996, AJ, 470, 364
Eigenbrod, A., Courbin, F., Vuissoz, C., et al. 2005, A&A, 436, 25E
Gaskell, C. M., & Peterson, B. M. 1987, ApJS, 65, 1
Giveon, U., Maoz, D., Kaspi, S., et al. 1999, MNRAS, 306, 637
Hook, I. M., McMahon, R. G., Boyle, B. J., & Irwin, M. J. 1994, MNRAS, 268, 305
Huchra, J., Gorenstein, M., Kent, S., et al. 1985, AJ, 90, 691
Irwin, M. J., et al. 1989, Nature, 338, 6218, 745
Koptelova, E., Shimanovskaya, E., Artamonov, B., et al. 2005, MNRAS, 356, 323
Koratkar, A. P., & Gaskell, C. M. 1989, ApJ, 345, 637
Koratkar, A. P., & Gaskell, C. M. 1991, ApJS, 75, 719
Lehár, J., Hewitt, J. N., Roberts, D. H., & Burke, B. F. 1992, ApJ, 384, 453
Oknyanskij, V. L. 1993, Pis'ma Astron. Zh., 19, 1021
Oknyanskij, V. L. 1999, Astron. Nachr., 320, 314
Oknyanskij, V. L., Lyuty, V. M., & Chuvaev, K. K. 1994, IAU Symp., 159, 401
Oknyanskij, V. L., Lyuty, V. M., Taranova, O. G., & Shenavrin, V. I. 1999, Astron. Lett., 25, 483
Østensen, R., Refsdal, S., Stabell, R., et al. 1996, A&A, 309, 59
Patnaik, A. R., & Narasimha, D. 2001, MNRAS, 326, 1403
Pelt, J., Kayser, R., Refsdal, S., & Schramm, T. 1996, A&A, 305, 97
Refsdal, S. 1964, MNRAS, 128, 307
Rix, H.-W., Schneider, D. P., & Bahcall, J. N. 1992, AJ, 104, 959
Slavcheva-Mihova, L. S., Oknyanskij, V. L., & Mihov, B. M. 2001, Ap&SS, 275, 385
Schmidt, R. W., Kundic, N., Pen, U.-L., et al. 2002, A&A, 392, 773
Schmidt, R., Webster, R. L., & Lewis, G. F. 1998, MNRAS, 295, 488
Schneider, D. P., Turner, E. L., Gunn, J. E., et al. 1988, AJ, 95, 1619; Erratum 1988, AJ, 96, 1755
Sergeev, S. G., Doroshenko, V. T., Golubinskiy, Yu. V., et al. 2005, ApJ, 622, 129
Shakura, N. I., & Sunyaev, R. A. 1973, AJ, 24, 337
Tikhonov, A. N., & Arsenin, V. Y. 1977, Solution of ill-posed problems (John Wiley and Sons)
Timmer, J., & König, M. 1995, A&A, 300, 707
Vakulik, V. G., Schild, R. E., Dudinov, V. N., et al. 2004, A&A, 420, 447
Wambsganss, J., & Paczynski, B. 1994, ApJ, 108, 1156
Wambsganss, J., Brunner, H., Schindler, S., & Falco, E. 1999, A&A, 346, L5
Woźniak, P. R., Alard, C., Udalski, A., et al. 2000, ApJ, 529, 88
Yee, H. K. C. 1988, AJ, 95, 1331
Zheng, W., Kriss, G. A., Telfer, R. C., et al. 1997, ApJ, 475, 469